Paper Received 4 October 2016, Received in revised form 24 May 2017,
Accepted 27 May 2017, Available online 2 June 2017

Published in Remote Sensing of Environment 202 (2017), pp. 152–165

http://dx.doi.org/10.1016/j.rse.2017.07.038

# Investigating Spatiotemporal Snow Cover Variability via an Improved Cloud-free MODIS Snow Cover Product in Central Alborz region.

Alireza B. Dariane[a],∗, Amin Khoramian[a], Emanuele Santi[b]

a Department of Civil Engineering, K.N. Toosi University of Technology, Tehran, Iran

b Institute of Applied Physics, National Research Council, Florence, Italy

## Abstract

Snow is a major source of different demands in Central Alborz Mountains. Hence, understanding snow spatial distribution and temporal variation is crucial for the management of water resources. Since . the in-situ measurements in the area are not sufficient, we referred to the MODIS snow cover products, whose capabilities in providing a spatially distributed and accurate mapping of snow are well demonstrated. In this analysis, we considered all the available MODIS acquisitions from both AQUA and TERRA satellites on the area, for a total of 4873 daily tiles of MOD10A1 and MYD10A1 with 500 meters spatial resolution, collected during the winter seasons between 2002 and 2015. The problem of cloud coverage, with set serious constraints to the snow mapping in the area, was addresses by developing an innovative sequential cloud removal algorithm, which applies different methods subsequently considering their temporal superiorities. To validate the algorithm, virtual cloud coverage with 25%, 50% and 75% probability of occurrence were added to images with least cloudiness. Then these images were used as ground truth. The results indicate that developed algorithm reduces cloud coverage by 94% and preserves accuracy of 93%. Next, to study snow cover spatiotemporal changes, different indices including snow cover duration (SCD), snow accumulation onset (*SAOD)* and melt ending dates (*SMED)* were calculated. Trend analysis (at 10% significance level) showed that 61% of areas between 2000 and 2300 m of elevation a.s.l. have reduction in SCD. SAOD is shifted forward in time and in contrary SMED is shifted backward in all basins. To investigate snow and temperature dependency, MODIS land surface temperature products were utilized. Results revealed that snow melt period and maximum snow cover are highly depended on temperature variations. Although study period (13 years) is not as long as needed for long-term inferences but outcomes indicate a severe snow cover reduction during recent years.

## 1- Introduction

Central Alborz (CA) region is a part of Alborz mountain range that is high elevated and is headwater of several rivers namely Haraz, Chaloos, Latian, Karaj, etc. These rivers supply water for about 21 million

people in downstream (Statistical Centre of Iran 2010), including the Iran capital, Tehran with 16 million populations.. Several dams operate CA for managing water for agricultural and municipal uses, and for generating hydropower. In CA, snow plays a key role in hydrologic cycle: accumulating in cold seasons and melting in warm seasons makes the snow a water bank which stores precipitation and releases it slowly afterwards. IPCC (acronym) reported that snow cover areas in northern hemisphere are reduced during recent decades (Bates et al 2008) and temperature rising due to global warming is expected in future (IPCC 2014). Also some signs of water scarcity that is expected in Iran by 2025 (The World Bank 2007) are seen in recent years, as the deficit in providing municipal uses and hedging in summer and agricultural drought in some basins are some of them. These facts causes some concerns about snow budget situation and its variations in CA. Clarifying this is crucial for better understanding about current situation and planning for future.

Snow distribution is mainly controlled by precipitation, temperature, radiation and topography, which vary drastically in mountainous regions (Dye and Tucker 2003; Tong et al 2008). In-situ measurements do provide punctual estimate of snow parameters, however, considering the spatial and temporal coverage needed to obtain reliable estimates, direct measurements can be extremely expensive or unfeasible in mountainous regions with a complicated orography such as CA. The development of remote sensing sensors has made it possible to study hydrological parameters in a quantitative way since 1980s. Hence, the possibility of using remote sensing techniques offers several advantages due to their ability to observe large areas in a very short time and measure integrated values of snow parameters instead of several sparse samples. Another consequence of these characteristics is the capability to monitor temporal trends of the observed parameters, thus improving prediction by hydrological models through use of repeated satellite passages. The potential sensors operating in the thermal, infrared and microwave regions of the electromagnetic spectrum for snow monitoring was well demonstrated, and several snow products derived from these sensors are freely available [ref. e.g. NSIDC]. Visible and near infrared bands allow mapping the snow cover extent and related parameters such as the snow cover persistence, with a moderate to high spatial resolution. Microwaves also allow the direct estimate of snow depth (SD) and snow water equivalent (SWE),but with a coarser resolution than optical sensors. Among the optical sensors currently in orbit, MODIS is one of the most popular in snow studies, due to its fine 500-meter spatial resolution, daily revisit time and a good scientific product developer team (Frei et al 2012). Visual (Visible?) and near infrared bands e MODIS sensor to observe snow cover onboard both Terra and Aqua satellites. Utilizing these bands, Normalized Difference Snow Index (NDSI) which is introduced by Dozier (1989) and developed by Hall et al (2002) is MODIS distinction tool to differentiate snow covered areas from other surfaces. A set of snow cover products including daily to monthly snow cover maps are provided by MODIS scientific team (Hall et al 2002). MOD10A1 and MYD10A1 are daily snow cover products with 500-meter

spatial resolution and daily frequency on Terra and Aqua satellites respectively. Many studies are investigated MODIs daily snow cover accuracy in different areas around the world (e.g. Klein and Barnet 2003; Maurer et al 2003; Ault et al 2006; Parajka and Blöschl 2006; Hall and Riggs 2007; Yang et al 2015). Most of studies show MODIS snow products have high accuracy in mapping snow cover. For instance, Klein and Barnet (2003) reported overall accuracy of 94% in comparison with SNOTEL stations in Upper Rio Grande river basin. Hall and Riggs (2007) showed 93% agreement against SNOTEL observations too. In addition, Yang et al (2015) indicated more than 91% accuracy for MOD10A1 and MYD10A1 in Tibetan Plateau. However, some errors due to thin snow (less than 1 to 4 cm) depth, forested regions and cloudy condition are reported as well (Klein and Barnet 2003; Maurer et al 2003; Ault et al 2006; Hall and Riggs 2007; Yang et al 2015).

Cloud obscuration due to cloud coverage in visible and near infrared wavelengths represents the major limitation of optical sensors for snow mapping, especially in mountainous areas which are frequently covered by clouds. This problem has been addressed by several studies (Tekeli et al 2005; McGuire et al 2006; Parajka and Blöschl 2006; Andreadis and Lettenmaier 2006; Wang et al 2009). Different methods have been developed to overcome this problem. Parajka and Blöschl (2008) presented a set of methods consist of combining Terra and Aqua images, Replacing cloud pixels by neighbor pixels, and using preceding days images to reduce cloud coverage. They assessed these methods accuracy against in situ measurements and found that 95.5%, 94.9% and 92.1% respectively. In addition, they stated that the methods accuracies depends strongly to the season. Snow accumulation and melting periods are most sensitive periods. Gafurov and Bardossy (2009) applied six successive methods for cloud reduction in Kokcha river basin in Afghanistan. They used snow-land transition elevations for first time, which was completed, and more developed by Parajka et al (2010) as regional snow-line method. This method is based on making decision about cloudy pixels above snow lines and under often cloud free elevations. Gafurov and Bardossy (2009) also presented a validation methodology for places with rare in situ observations. They borrowed cloud mask from a cloudy image and applied it on a clear sky image. Then the original cloud free image was used as ground truth for new cloud added one. This validation methodology used in later studies such as Paudel and Andersen (2011) and modified by Da Ronco and De Michele (2014). Using passive microwave (PM) sensors cloud penetration ability, evaluated by Gao et al (2010). They used AMSRE snow water equivalent product (AE_DySno) along with combining Terra and Aqua MODIS snow covers and temporal combination. Although AMSRE products are cloud free but its low spatial resolution (25 Km) limits its application and cause large errors in cloud removal. In Gao et al (2010) study, produced cloud free product accuracy is reached to 79% which is mainly due to using AMSRE. Also Mhawej et al (2014) used AMSRE. The accuracy of cloud-free product are found to be equal to 85% for their study area, Lebanon. Different methods and sequence of them have been utilized to reduce cloud obscuration until

now. But a key question is still remained which rises from Parajka and Blöschl (2008) statement that said the methods accuracy is highly seasonal. In all studies, sequence of algorithms is same for all seasons and there is no clear idea behind in arrangement of methods. Here we focused on this matter and tried to propose a method that accounts seasonal superiority of methods. Also we modified validation methodology that presented by Gafurov and Bardossy (2009) and modified by Da Ronco and De Michele (2014) to make it more robust and reasonable. We suggested a methodology to select cloud masks and clear sky images to account different cloud patterns.

Different indices are used to investigate snow cover spatiotemporal changes in studies (Tang 2013; Tahir et al 2014; Wang et al 2014a; Gascoin et al 2015; Marchane et al 2015; Mir et al 2015). Most popular indices are snow cover duration (SCD), snow cover percentage (SCP) and snow onset and melt dates. We utilized these indices and defined other indices that extracted from snow depletion curves (SDCs) in each hydrological year. Indices trends in time are analyzed and theirs significance evaluated by hypothesis tests. To investigate snow relativity to temperature that is most important climate change indicator we utilized MODIS monthly land surface temperature (LST) product namely, MOD11C3 (Wan, 1999). Several studies indicated that MODIS LST could be a good proxy of air temperature (Jin and Dickinson 2010; Mildrexler et al 2011; Van Nguyen et al 2015). Also recently, Shamir and Georgakakos (2014) used MODIS LST as snow modeling forcing and their results showed MODIS LST could perform well.

The aim of this paper is to investigate spatiotemporal snow cover changes using different indices and evaluate its relativity to temperature as climate change indicator. To do this an innovative cloud removal algorithm is developed to reduce cloud cover as much as possible and remain accuracy as well as original images by accounting temporal and local superiority of different removal methods. Using cloud removed snow products snow cover spatiotemporal changes is studied and its trend in time is analyzed statistically. To investigate snow cover-temperature dependencies MODIS LST is implemented too and their pair correlation is evaluated.

## 2- Study area and data Sets

### 2-1- Study area

Central Alborz (CA) region is located in the north of Iran and in the middle of Alborz range. CA region covers 26845 $Km^2$ area and its elevation ranges between 0 to 5604 m above sea level (a.s.l.). CA is subdivided to two main sub domains. Northern sub domain climate is categorized as warm and humid: it is

mainly influenced by Caspian Sea moist airflows and it is characterized by orographic precipitation and high cloud persistency. The Alborz range blocks passage of moist air and creates an arid region in the lee side. In southern sub domain, precipitation is mainly due to west to east airflows that mostly originate from Mediterranean Sea. Long-term annual precipitation is 294 mm per year in Tehran province which is located in southern domain and is 703 and 896 mm per year at Guilan and Mazandaran provinces in northern sub domain (IRIMO 2014). CA is composited of nine basins (Table 1) that are shown in Figure 1.

**Table 1- Study area and basins physiographic characteristics**

| | Area ($Km^2$) | Minimum Elevation (m) | Maximum Elevation (m) | Mean Elevation (m) | Mean Hypsometric Elevation (m) |
|---|---|---|---|---|---|
| **Taleghan** | 947.207 | 1730 | 4394 | 2672.7 | 2645 |
| **Chaloos** | 1658.835 | 108 | 4275 | 2040.3 | 2039 |
| **FiroozKuh** | 2535.365 | 1458 | 4048 | 2465.0 | 2415 |
| **Haraz** | 4064.127 | 199 | 5604 | 2654.2 | 2758 |
| **Karaj** | 843.9928 | 1710 | 4343 | 2834.9 | 2802 |
| **Lar** | 733.2647 | 2532 | 5597 | 3120.0 | 3085 |
| **Latian** | 700.9325 | 1609 | 4300 | 2566.8 | 2533 |
| **Mamloo** | 1770.519 | 1241 | 4300 | 2229.0 | 2133 |
| **Sehezar** | 941.1879 | 74 | 4761 | 2177.6 | 2312 |
| **Study area** | 26845.22 | 0 | 5604 | 2056.5 | 2102 |

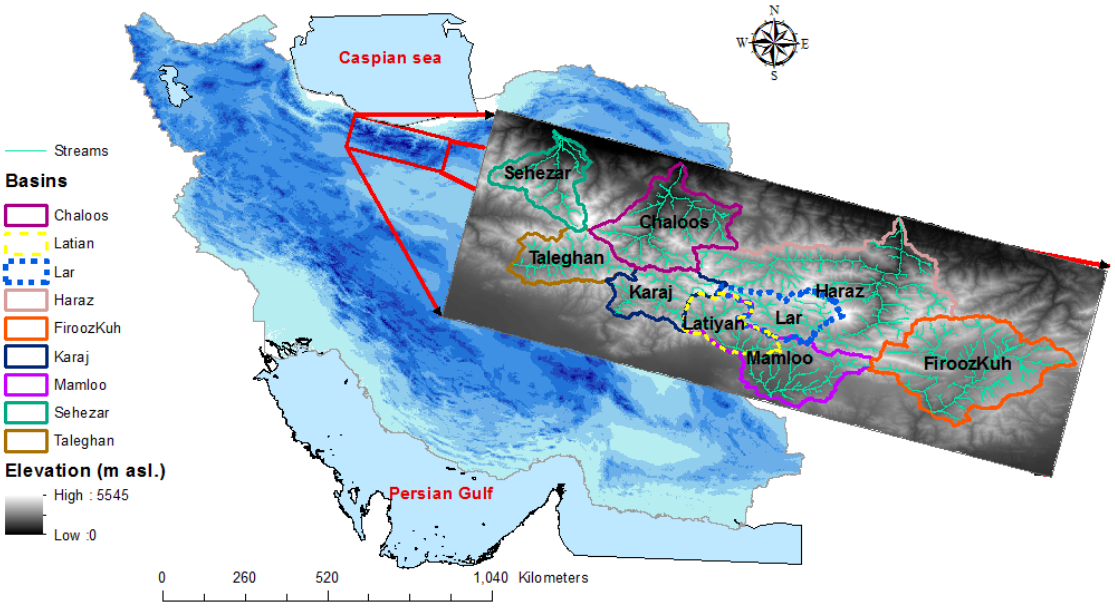


**Figure 1- Study area**

## 2-2- Snow Cover

MODIS on Terra and Aqua daily snow cover products (MOD10A1 and MYD10A1, respectively) version 5 are used in this study. 500 m resolution daily snow cover datasets are provided in tiles of 10°x10° approximately at the equator with sinusoidal projection and are stored in Hierarchical Data Format (HDF). Our test area corresponds to the H22v05 tile . A total of 4837 H22v05 tiles, covering the in period from 1 October 2002 to 31 September 2015, were obtained through NASA's earth observing system data discovery tool via "Reverb" website (http://reverb.echo.nasa.gov). Detailed information on MODIS SCPs snow cover retrieval algorithm is available at Hall et al (2002). In brief, snow high reflectance in visible wavelength and absorption in shortwave infrared is used to develop Normalized Difference Snow Index (NDSI) for snow cover detection. NDSI is normalized difference of visible and shortwave infrared bands reflectance.

$$NDSI = \frac{R_v - R_{si}}{R_v + R_{si}} \quad R_v = \text{visible reflectance} \quad R_{si} = \text{shortwave infrared reflectance}$$

Employing this index and some other constraints, SNOWMAP algorithm is adopted for retrieving snow cover in MODIS SCPs.

### 2-3- Digital Elevation Model (DEM)

Topographic information is derived from The Advanced Spaceborne Thermal Emission and Reflection Radiometer (ASTER) Global Digital Elevation Model (GDEM) version 2. ASTER GDEM provides global coverage with 30 m resolution (METI and NASA, 2011). Eight tiles (N35E050, N35E051, N35E052, N35E50, N36E50, N35E51, N36E52 and N36E52) are downloaded from Reverb and then mosaicked to cover study area. Basin boundaries and streams map are extracted from DEM data and then resampled via bilinear method to match MODIS snow cover 500 m resolution, in order to produce an aspect map, which is needed for cloud removal methods and further analyses.

### 2-4- Land surface temperature (LST)

Due to the absence of dense in situ measurements and to the data distribution policy in Iran, MODIS/Terra monthly land surface Temperature (MOD11C3, Version 5) is used to investigate temperature dependencies. MODIS monthly LSTs represent monthly averaged land surface temperature using daily products (MOD11A1) in clear sky conditions at 0.05-degree resolution. Previous studies showed that MODIS LSTs work well in order to snow modeling in ungaged regions (Shamir and Georgakakos 2014). A total of 156 images in study period are downloaded via "Reverb" website. LSTs are preprocessed to obtain basin wide temperatures at Celsius unit. The LSTs digital numbers (DNs) in 16bit are converted into Celsius and then gridded and averaged on every basin..

## 3- Methodology

### 3-1- Cloud Removal Algorithm

Our cloud removal algorithm is based on benefiting advantages of different methods in a united framework. We emphasized on localizing methods including Terra and Aqua combination, snow line filtering, using neighbor pixels and time filtering in our case and combining them to each other considering theirs temporal accuracies. This strategy is to reduce cloud as much as possible while preserving accuracy well. In this section, used methods and combining strategy are described respectively. Finally, Validation methodology and its refinements are given.

#### 3-1-1- Terra and Aqua combination

About three hours difference between MODIS\Terra and Aqua overpass time may let clouds to move and uncover land surface. That's why combining these sensors is frequently used in different studies (Parajka and Blöschl 2008; Gafurov and Bardossy 2009; Gao et al 2011; López-Burgos et al 2013; Da Ronco and De Michele 2014). We applied this method by giving priority to MOD10A1 observations. When these pixels are covered by clouds, MYD10A1 observations are used instead. In this way, if a pixel is classified as cloud in MOD10A1 and be cloud-free (snow or land) in MYD10A1, no cloud observation would be replaced. MOD10A1 priority is due to validation studies such as Yang et al (2015), which demonstrate its more accurate retrievals than MYD10A1. It is mainly due to operational problem in Aqua band 6, which forces to use band 7 instead (Hall and Riggs 2007). To have a better understanding about this method ability to reduce cloud obscuration, seasonally averaged difference between two sensors is mapped in figure 2-c. This map shows number of days (in percent) which cloud classification differs. Basin averaged values (Table 2) indicate more differences in summer and spring seasons. Therefore, it means combining Terra and Aqua images could be more effective in spring and summer.

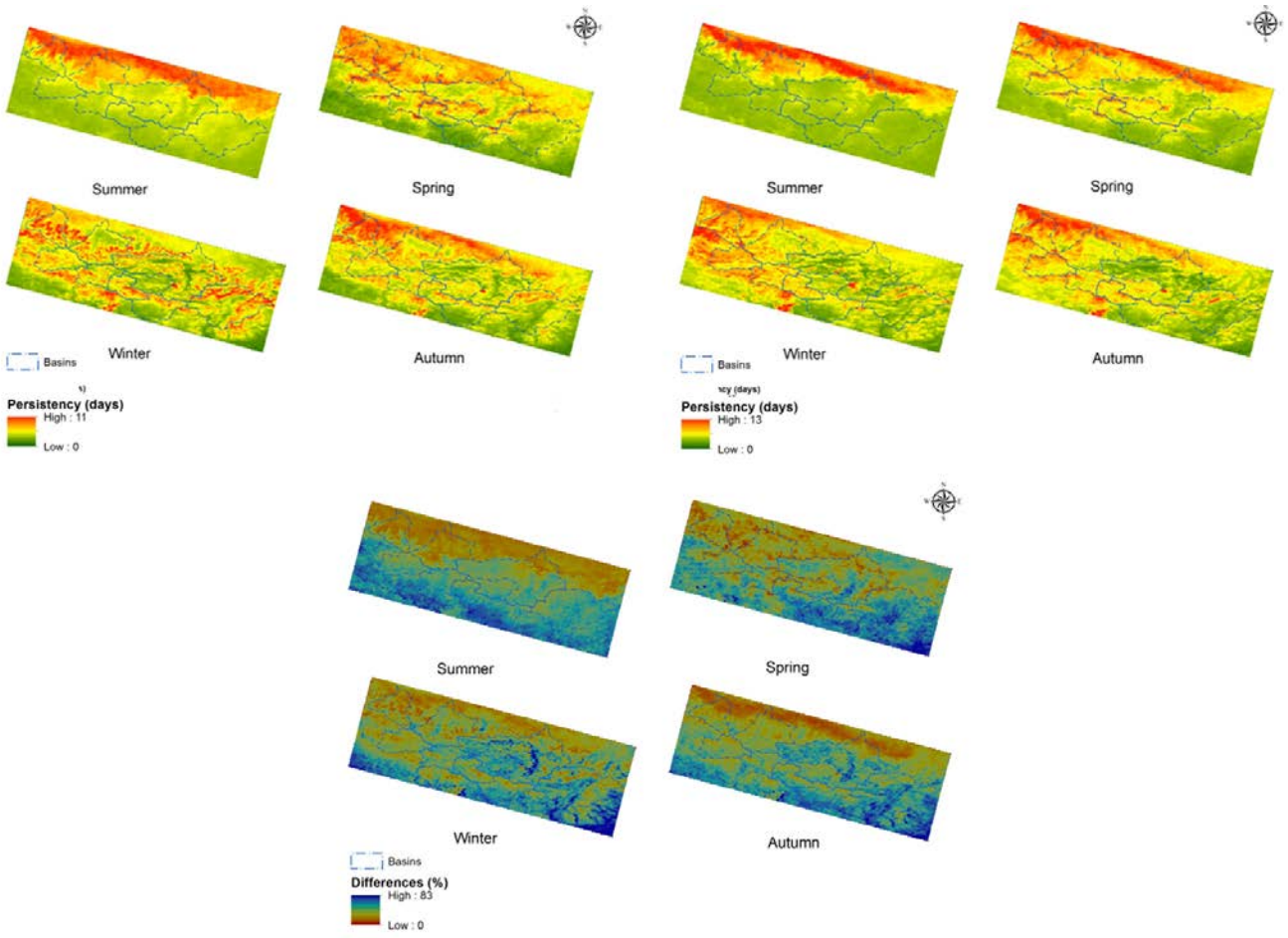


193

194 **Figure 2. Cloud persistency index for a) Aqua sensor and b) Terra sensor and c) Averaged difference in Terra and Aqua**
195 **(%)**

196

197 **3-1-2- Time Filtering**

198 Time filtering is one of the most popular methods in cloud reduction studies (Parajka and Blöschl 2008;
199 Huang et al 2014; Wang et al 2014b; Da Ronco and De Michele 2014). This method uses observations in
200 the preceding and the antecedent days. Actually, this method assumes that land surface condition (snow or
201 land) do not change in the considered time window. It is clear that as large is the time window, as large is
202 the error caused by this assumption. . Thus, the effective time window size is defined as tradeoff between
203 the reduction of cloud cover effects and the error due to the method assumption. To discover the effective
204 time window size, cloud persistency index (CPI) is defined and calculated. This index is obtained by
205 averaging duration of the days, in which continuous cloud persistency is present. For example if 3 cloudy
206 events (continuous cloudy days) with 3, 4 and 5 days durations are given, CPI would be equal to 4. Figures
207 2-a and 2-b show mapped cloud persistency index for Terra and Aqua respectively. More cloud persistency

is obvious in north domain in comparison to south domain, especially in summer. The reason as described in section 2 is due to moist airflows, which come from Caspian Sea. Basin averaged values (Table 2) indicate CPI average in most cases do not exceeds form 4 days. Also, to be able to use developed method for real time and hydrological modeling purposes, only preceding days are used. Therefore, we used a 4 days backward time filtering. For a cloudy pixel, this method searches until 4 preceding days to find a no-cloud observation and subsequently replaces it.

**Table 2. Cloud Persistecy Index and averaged differene in Terra and Aqua cloud observations values**

| | Terra Cloud Persistency Index (days) | | | | Aqua Cloud Persistency Index (days) | | | | Averaged Difference (%) | | | |
|---|---|---|---|---|---|---|---|---|---|---|---|---|
| **Basins** | **Spring** | **Summer** | **Autumn** | **Winter** | **Spring** | **Summer** | **Autumn** | **Winter** | **Spring** | **Summer** | **Autumn** | **Winter** |
| **Chaloos** | 2.43 | 2.35 | 2.35 | 2.73 | 2.36 | 2.45 | 3.02 | 3.51 | 28.07 | 24.96 | 13.53 | 13.59 |
| **FiroozKuh** | 1.81 | 1.32 | 2.07 | 2.37 | 1.98 | 1.60 | 2.62 | 3.63 | 35.22 | 46.11 | 20.42 | 16.57 |
| **Haraz** | 2.13 | 1.64 | 2.11 | 2.38 | 2.18 | 1.87 | 2.62 | 3.14 | 30.82 | 37.31 | 18.13 | 17.15 |
| **Karaj** | 2.22 | 1.42 | 2.37 | 2.93 | 2.20 | 1.59 | 2.81 | 3.38 | 30.69 | 45.22 | 16.98 | 15.99 |
| **Lar** | 2.34 | 1.48 | 2.34 | 2.42 | 2.30 | 1.67 | 2.75 | 2.76 | 29.78 | 41.34 | 16.93 | 18.97 |
| **Latian** | 2.21 | 1.42 | 2.39 | 2.78 | 2.16 | 1.52 | 2.84 | 3.64 | 32.16 | 46.44 | 17.12 | 15.08 |
| **Mamloo** | 1.80 | 1.30 | 2.10 | 2.36 | 1.78 | 1.36 | 2.39 | 3.09 | 37.31 | 55.07 | 20.73 | 17.44 |
| **Sehezar** | 2.71 | 2.31 | 2.67 | 3.19 | 2.50 | 2.54 | 3.65 | 4.22 | 27.32 | 25.41 | 11.36 | 11.33 |
| **Taleghan** | 2.20 | 1.40 | 2.45 | 3.04 | 2.17 | 1.58 | 2.83 | 3.49 | 31.34 | 41.53 | 15.19 | 13.60 |

### 3-1-3- Using Snow Line

Parajka et al (2010) reclassifies cloudy pixels deriving information from snow altitudinal variations. To do this, two snowline (SnowL) and landline (LandL) elevations have to be found. SnowL is defined as the mean elevation of pixels classified as snow and it is used to reclassify cloudy pixels at an elevation above SnowL as snow. LandL is similarly mean of land (free of snow) pixels elevations. If cloudy pixel elevation is below landline, it is classified as land. To account snow and land lines variations across different aspects due to solar radiation, SnowL and LandL are calculated for 4 aspects separately. Using DEM, study area categorized to 4 aspects including north, east, south and west. Then, method is applied for each one separately. The method fails estimating snow and land lines correctly in case of high cloud coverage in the image. In this case, the estimation may be unrealistic since it is based on few cloud free pixels. as According to Parajka et al (2010) the method was not applied if more than 70% of the image is covered by clouds. If the coverage is below this threshold, the method estimates SnowL and LandL and the cloudy pixels are reclassified as follows:

1- Cloudy pixel is assigned as snow, if is above SnowL
2- Cloudy pixel is assigned as land, if is below LandL
3- Cloudy pixel is remained unchanged, if is between SnowL and LandL

### 3-1-4- Using Neighbor pixels

This method is based on instance based learning theorem (Mitchell 1997). It is utilizing surrounding pixels information to decide about cloudy pixels. Considering k neighbor pixels, which are surrounding a cloudy pixel, if a neighbor pixel is located at higher elevation and is snow covered, a score is added to target function. Contrariwise, if a neighbor pixel is below cloudy pixel and is classified as land, a score is subtracted. Finally if target function value is more than zero, cloudy pixel is reclassified as snow. In contrary, negative target function value corresponds to reclassifying cloudy pixel as land. If target function is equal to zero, no decision is made. This method could be formulized as follows to reclassify a cloudy pixel located at x and y.

$$\delta(m,n) = \begin{cases} +1 & if \quad Elevation(m,n) \le Elevation(x,y) \quad and \quad Class(m,n) = Snow \\ 0 & Otherwise \\ -1 & if \quad Elevation(m,n) \ge Elevation(x,y) \quad and \quad Class(m,n) = Land \end{cases}$$

$$f(x,y) = \sum_{i=-n}^{n} \sum_{j=-n}^{n} \delta(x+i, y+j) \qquad i \neq 0 \;\&\; j \neq 0$$

$\delta(m,n)$ and $f(x,y)$ are scoring and target functions respectively. We investigated this method considering 8 and 24 neighbors (Figure 3). In target function, n would be equal to 1 and 2 for 8 and 24 neighbors respectively. Also we added another constraint to scoring function to account aspects variations too. It is so that score function would be applied for pixels, which are in a same aspect as cloudy pixel. Therefore scoring function formulation would be as follows:

$$\delta(m,n) = \begin{cases} 1 & if \quad Elevation(m,n) \le Elevation(x,y) \quad and \quad Class(m,n) = Snow \quad and \quad Aspect\ (m,n) = Aspect(x,y) \\ 0 & Otherwise \\ -1 & if \quad Elevation(m,n) \ge Elevation(x,y) \quad and \quad Class(m,n) = Land \quad and \quad Aspect\ (m,n) = Aspect(x,y) \end{cases}$$

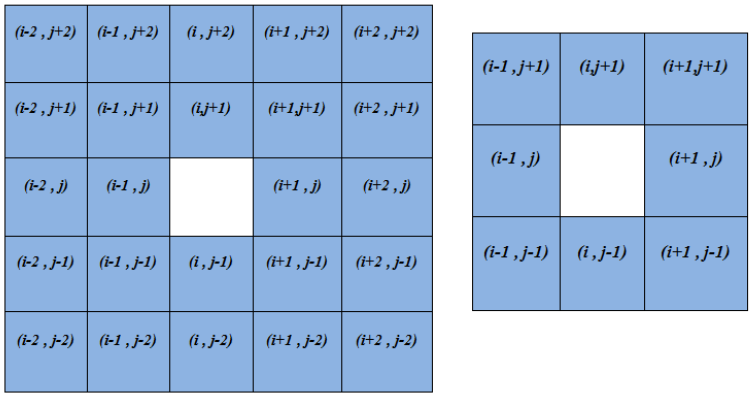


**a)** **b)**

**Figure 3. Surronding pixels considering a) 25 neighbors and b) 8 neighbors**

### 3-1-5- Combining Algorithm

The cornerstone of the combining algorithm is considering following facts: 1- Using more cloud removal methods causes much error 2- Methods accuracies differ temporally. Actually, this algorithm tries to remove clouds using most accurate methods at first and if any cloud is remained, uses other methods. The reason of such strategy is to edit images as little as possible to avoid decreasing accuracy. To aim this, methods accuracies are assessed in every month. Then, they are prioritized based on accuracies and a list of ranked methods for every month is prepared. If images cloudiness is higher than 5% (Clear sky threshold), image is entered in cloud reduction algorithm. Algorithm steps are summarized below:

1- Imagery month is determined.

2- Using step 1, first rank cloud removal method (considering accuracy) is applied and then the method is removed from ranking list.

3- Cloudiness is calculated.

4- If cloudiness is less than 5%, Algorithm goes to next image, otherwise goes to step 2.

### 3-1-6- Validation Methodology

Obviously, the best way to validate the proposed cloud removal method is using in situ measurements as ground truth; however, for CA area extensive and continuous stations records are unavailable. Therefore, another methodology has been set up, which borrows the cloud coverage from a highly clouded image and

fills a cloud free image using that. Thus, cloud free image is considered as ground truth for corresponding cloud-filled one. The accuracy assessment results may depend on the selection of cloud masks and the number of cloud free images to be validated; therefore, we focused on developing an unbiased procedure, in order to obtain more reliable results. For example Parajka and Blöschl (2008), Paudel and Andersen (2011) and Da Ronco and De Michele (2014) used 2, 10 and 25 images for validation, respectively. In these studies, the number of validation images and selection of cloud mask did not rely on any specific reason. Here, the following procedure is proposed: for every month of the 13 years studying period, the most clear day is chosen, thus obtaining 156 cloud free images. ,. Using other images cloud mask ensures that the fictitious cloud mask would be similar to which occur in real. But, which image cloud mask does represent real condition? Selecting a highly clouded mask could be a choice as is so in mentioned studies, but it might not be which often occurs. To address this issue, we derived 25%, 50% and 75% probability of cloudiness occurrence (25PE, 50PE and 75PE, respectively) using cumulative distribution functions (CDFs) for every month (Figure 4). Occurrence probabilities are shown in table 3. Then, nearest images in cloudiness to 25PE, 50PE and 75PE within every month are found and their cloud masks are extracted. Therefore, every clear sky image, is associated with three cloud masks, for a total of 468 cloud-filled images. Hereafter, for better denotation, every cloud-filled image would be called using three indexes including l, m and y, which corresponds to level of cloudiness (25PE, 50PE and 75PE) and imagery month and year, respectively.

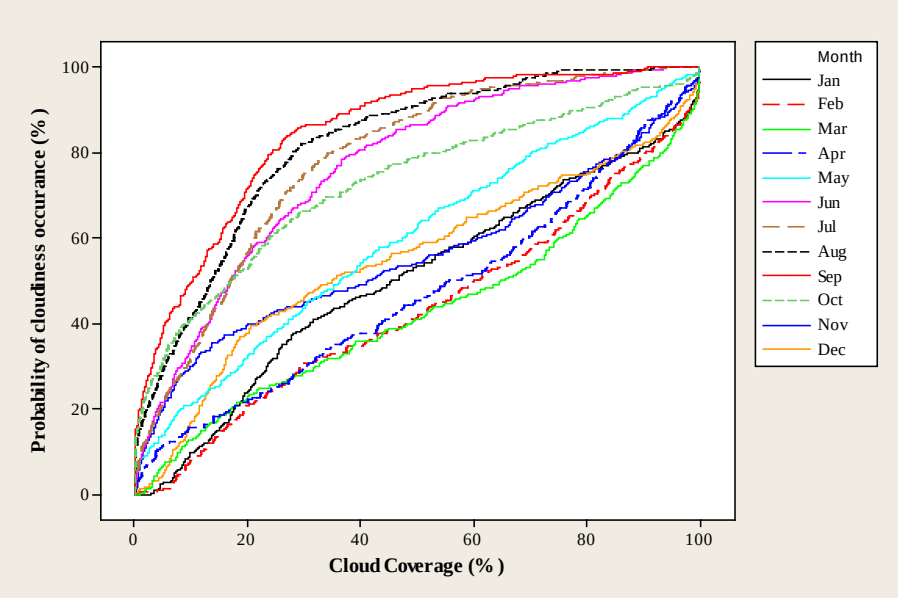


**Figure 4. Cumulative distribution function of cloudiness in different months**

296 **Table 3. cloudiness with 25%, 50% and 75% probability of occurance (%) in every month**

| Probability of occurrence | Jan | Feb | Mar | Apr | May | Jun | Jul | Aug | Sep | Oct | Nov | Dec |
|---|---|---|---|---|---|---|---|---|---|---|---|---|
| **%25** | 21 | 25 | 24 | 25 | 14 | 7 | 6 | 4 | 2 | 3 | 7 | 13 |
| **%50** | 46 | 60 | 65 | 56 | 36 | 17 | 17 | 14 | 10 | 17 | 42 | 35 |
| **%75** | 79 | 85 | 89 | 82 | 66 | 35 | 30 | 25 | 21 | 43 | 79 | 80 |

297

298 After applying cloud removal methods to the artificially cloud filled images and comparing resulting images
299 with corresponding ground truths, the accuracies are calculated. Let “a” be number of pixels reclassified
300 correctly (snow to snow and land to land pixels) and “b” be the number of pixels misclassified (Snow to
301 land and land to snow pixels). These values are computed for every image and used for time series analysis.
302 Hence, degree of agreement (DA) as a measure of accuracy is defined as percent of correctly reclassified
303 cloudy pixels in each image and is calculated as

304 $$DA_{b,l,m,y} = a_{l,m,y}a_{l,m,y} + b_{l,m,y}$$

305 Where l, m and y are image indexes.

306 Two steps are done to derive DA for each month. At first DAs are averaged along cloudiness levels. For
307 every validation image, a weight is calculated as the number of reclassified pixels over every basin.

308 $$w_{l,m,y} = a_{l,m,y} + b_{l,m,y}$$

309 Using this weight,

310 $$DAL_{m,y} = \frac{\sum_{l=1}^{3} w_{l,m,y} \times DA_{l,m,y}}{\sum_{l=1}^{3} w_{l,m,y}}$$

311 Where DAL is averaged DA in each month and year. Then, degree of agreement is found over entire study
312 period (13 years). Weights are defined as

313 $$WL_{m,y} = \sum_{l=1}^{3} w_{l,m,y}$$

314 Finally, overall degree of agreement is calculated as:

315 $$DAO_{m} = \frac{\sum_{y=1}^{13} WL_{m,y} \times DAL_{l,m}}{\sum_{l=1}^{3} WL_{m,y}}$$

316 DAOs are used for evaluating methods temporally superiorities.

317

318 **3-2- Snow Cover Metrics**

319 Various indexes are utilized to investigate snow cover changes. One of the most popular indexes is snow
320 cover duration (SCD), which is used in several recent studies (Brown et al 2007; Marchane et al 2015;
321 Wang et al 2015): SCD is the number of snow covered days in the given period. Here, interannual SCD
322 variations are investigated. In addition to SCD, some indices are derived from snow depletion curves
323 (SDCs). SCDs are extracted plotting snow cover percentage changes over a basin against day number (1-
324 365 or 366 for leap years). Hence, for every basin 13 SCDs are achieved. To avoid short-term snow cover
325 variations, 5 days moving averaged SDCs are used instead. Figure 5 shows a sample SDC and defined
326 indices, which are introduced below:

327 - *Maximum snow cover (MSC)* is maximum snow cover extent, which would be observed in a
328 hydrological year and could be an indicator of stored snow in the basin. In addition, the day
329 corresponds to *MSC* is named as *Maximum Snow Cover Day (MSCD).*
330 - *Snow Accumulation Period (SAP)* is the period from starting accumulation of snow to reach
331 maximum snow cover extent. The ratio of *MSC* to *SAP* is the rate of reaching to maximum snow
332 cover, which is called here as *Snow Accumulation Slope (SAS)*.
333 - *Snow Melt Period (SMP***)** is the period from maximum snow cover extent date to ending snow
334 budget in basin. This period indicates how long does it take to stored snow in basin be melted
335 completely. Melting rate would be characterized as *Snow Melt Slope (SMS)*.
336 - *Snow Accumulation Onset Day (SAOD***)** is snow accumulation starting day number. Actually, it is
337 the day, which is cold enough to incoming precipitation over basin being stored as snow. Delay in
338 precipitation and/or raise in air temperature in corresponding days could postpone *SAOD*.
339 - *Snow Melt Ending Day (SMED)* is the day, which snow storage in basin would be finished. *SMED*
340 is depended on snow volume that is stored in previous months and air temperature in melt season.
341 - *Accumulation-Ablation Period (AAP)* is the period between the day snow cover percentage exceeds
342 5% and remains more than 5% for 10 days to the day that SCP goes under 5% and continues to 10
343 days afterwards.
344 -

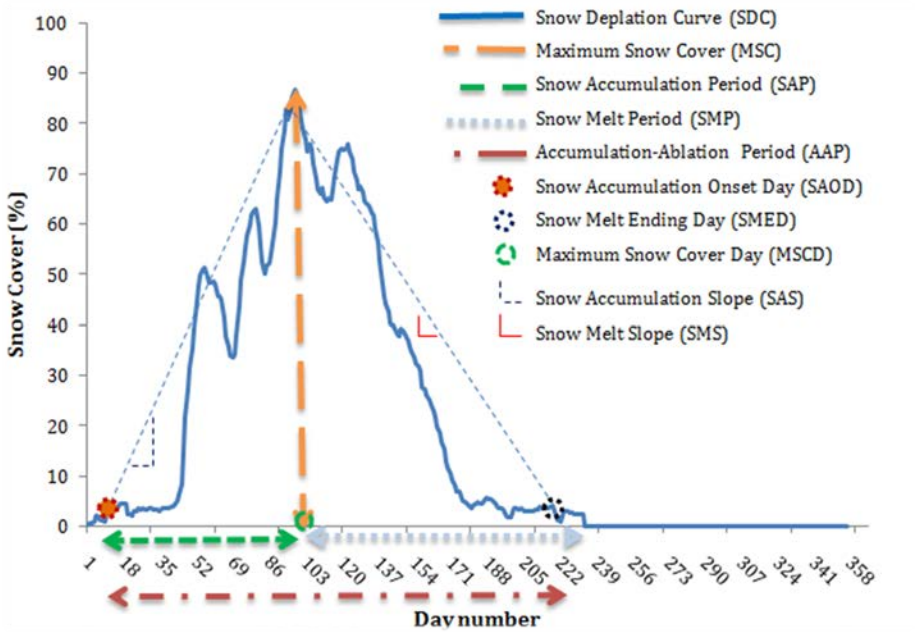


**Figure 5. A sample snow cover depletion curve (SDC) and determined snow indexes**

### 3-3- Analysis of Snow Indexes Time Series

A linear regression test is applied to identify the interannual trend of indexes time series. The slope of least square lines fitting the annual indexes values in every basin is calculated. Positive slope values show an increasing trend and negative values show a decreasing trend. In addition, to measure significances, p values are obtained using t-student test.

Pearson's r and Kendall's Tau are used to measure non-monotonic and monotonic correlation with land surface temperature respectively. When there is a linear correlation, Pearson's r would be a good measure. But in the cases that data are associated in a nonlinear pattern, Kendall's Tau, which is a rank based measure is a better choice. Further details can be found in (Helsel and Hirsch 2002)

## 4- Results and Discussions

### 4-1- Cloud Removal Algorithm

Applied methods are investigated through efficiency and accuracy criteria. 1) Methods efficiencies in removing clouds are calculated as rate of cloud-removed pixels number to all cloudy pixels number. 2) Methods accuracies are assessed using described methodology in section 3-1-6. These criteria are presented in figure 6 for different applied methods. Multi sensor method accuracy is not considered due to assuming

that snow cover would not change in time shift between two sensors overpass time. As is shown in figure 6-a, cloud removal efficiency of multi sensor method is less than 10% in September to October. Unlike multi sensor method, time filtering is able to reduce cloud obscuration more than 80% in most months, although this method accuracy is low especially in snow accumulation months (November to February). Snow line method is applied in two forms. One time by considering different snow and land lines in aspects and second time without considering aspects variations. The efficiencies and accuracies of both forms are shown as “simple snowline” and “snowline with aspect” in figure 6-b respectively. Snow line considering aspects variations is more accurate than simple snowline, while cloud reduction in simple snowline exceeds considering aspects about 10% approximately. As illustrated in section 3-1-4 using neighbor pixels is adopted utilizing 8 and 24 surrounding pixels with and without involvement of aspects. Hence, four modifications of this method are applied. As results indicate, using 24 neighbors decreases cloud obscuration obviously in comparison to using 8 neighbors. In addition, aspects involvement reduces cloud removal efficiency, while does not cause a considerable accuracy improvement. Therefore, we discarded the implementations that include the aspect and we utilized both 8 and 24 neighbors in combining step. An interesting fact is the seasonal dependency of all methods accuracies. As figure 6 clearly points out, the accuracy decreases in snow accumulation months and increases while snow cover is reaching to its maximum and starts disappearing. This trend is more obvious in figure 7. White bars show long-term snow coverage. It is mainly due to difficulties in differentiating snow covered and land pixels while snow is accumulating. Rapid changes in snow condition and spatial and temporal confusion are more expected in these months. Using accuracy assessment results, methods are inter-compared to be prioritized and then be applied subsequently in combination step.

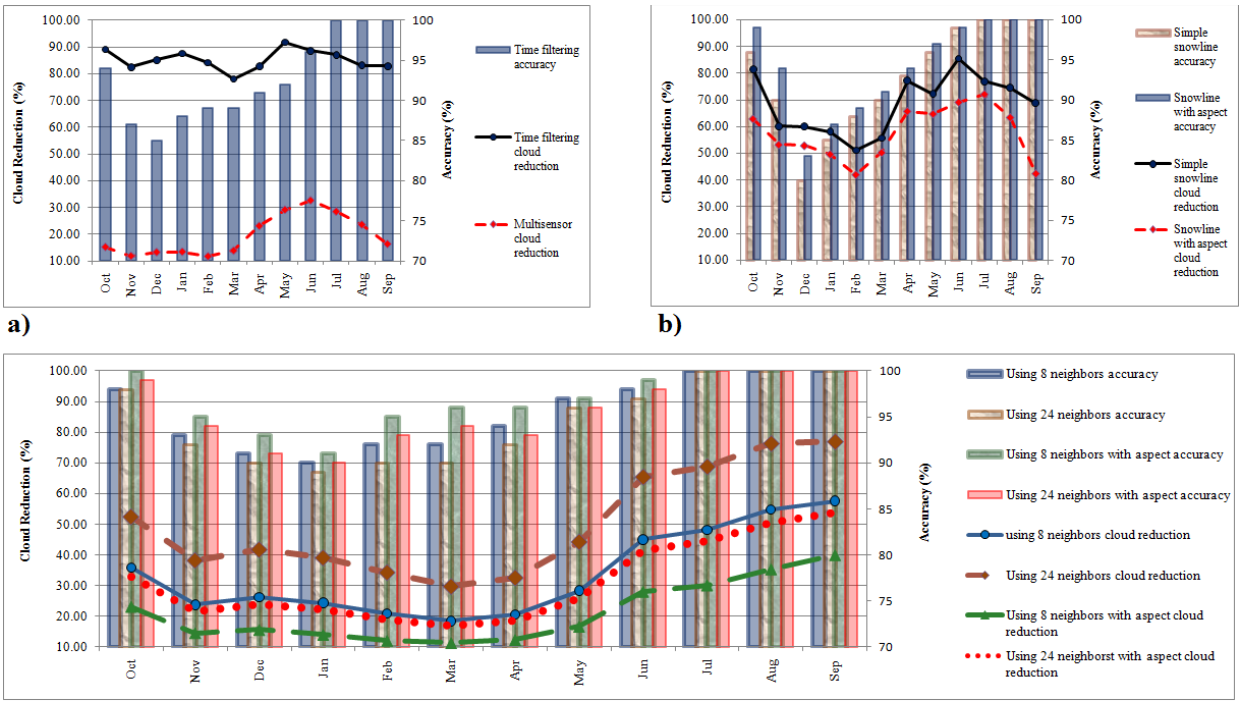


**Figure 6. Applied methods efficiency in cloud reduction and their accuracies a) snowline method b) Simple using neighbors method c) Using neighbors considering aspect d) Multi sensor and time filtering methods.**

Accuracy assessment results (Figure 7) show that snowline method (both with aspect and simple) accuracy decreases in December and January drastically and goes under time filtering accuracy. It means this method is not able to find accurate snow and land lines in these months and large errors would be made if this method is applied. While this method is most accurate one in October and November which months that snow coverage is less than 30% in long–term. In addition, it seems that in summer most of methods work well and there is no difference between them in accuracy. It is due to absence of snow that eases finding correct pixels coverage. By ordering sequence of methods by these results in every month and applying them until reach desired cloud coverage, combining step is done. As is shown, (Green dots in Figure 7) the combined methodology is able to preserve the accuracy of the best methods (8 neighbors?) but avoiding the large errors that affect some methods in the period from November to February. Table 4 is listed combined methodology accuracy and cloud reduction in each month.

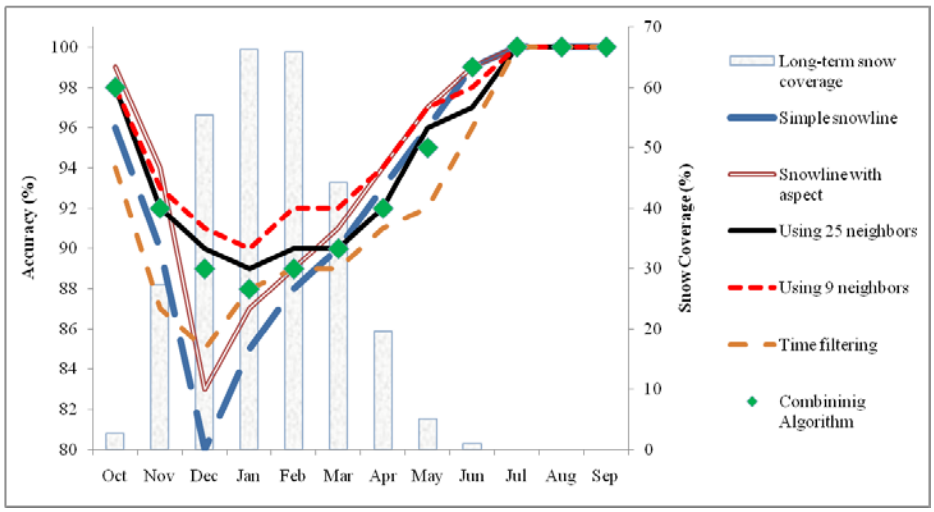


401

402 **Figure 7. Comparison of combining algorithm accuracy to used methods**

403

404 **Table 4- Combining method accuracy and cloud coverage before and after cloud reduction**

| | | Oct | Nov | Dec | Jan | Feb | Mar | Apr | May | Jun | Jul | Aug | Sep | Yearly |
|---|---|---|---|---|---|---|---|---|---|---|---|---|---|---|
| **Accuracy (%)** | | 98 | 92 | 89 | 88 | 89 | 90 | 92 | 95 | 99 | 100 | 100 | 100 | 93 |
| **Cloud cover (%)** | **Raw images** | 27.1 | 44.4 | 43.6 | 49.9 | 57.5 | 57.7 | 51.3 | 39.8 | 23.1 | 21.5 | 18.1 | 16.7 | 37.6 |
| | **Cloud reduced** | 1.0 | 3.6 | 2.7 | 1.7 | 5.5 | 6.7 | 4.3 | 1.1 | 0.6 | 0.6 | 0.6 | 0.2 | 2.4 |

405

406 ## 4-2- SCD variations

407 As it was illustrated in section 3-3, annual snow cover duration is calculated in every pixel over study area.
408 Then, using linear regression, trend coefficients are obtained. Figure 8-a shows mapped SCD trend
409 coefficients in study period (13 years). Trend coefficients vary from -6 to +2. It means that snow cover
410 duration is changed with a rate of between -6 to +2 days per a year in the study domain. To find significant
411 variations, p-values are obtained and mapped (Fig. 8-b) and pixels with significant SCD changes at 10%
412 significant level are specified (Fig 8-c).

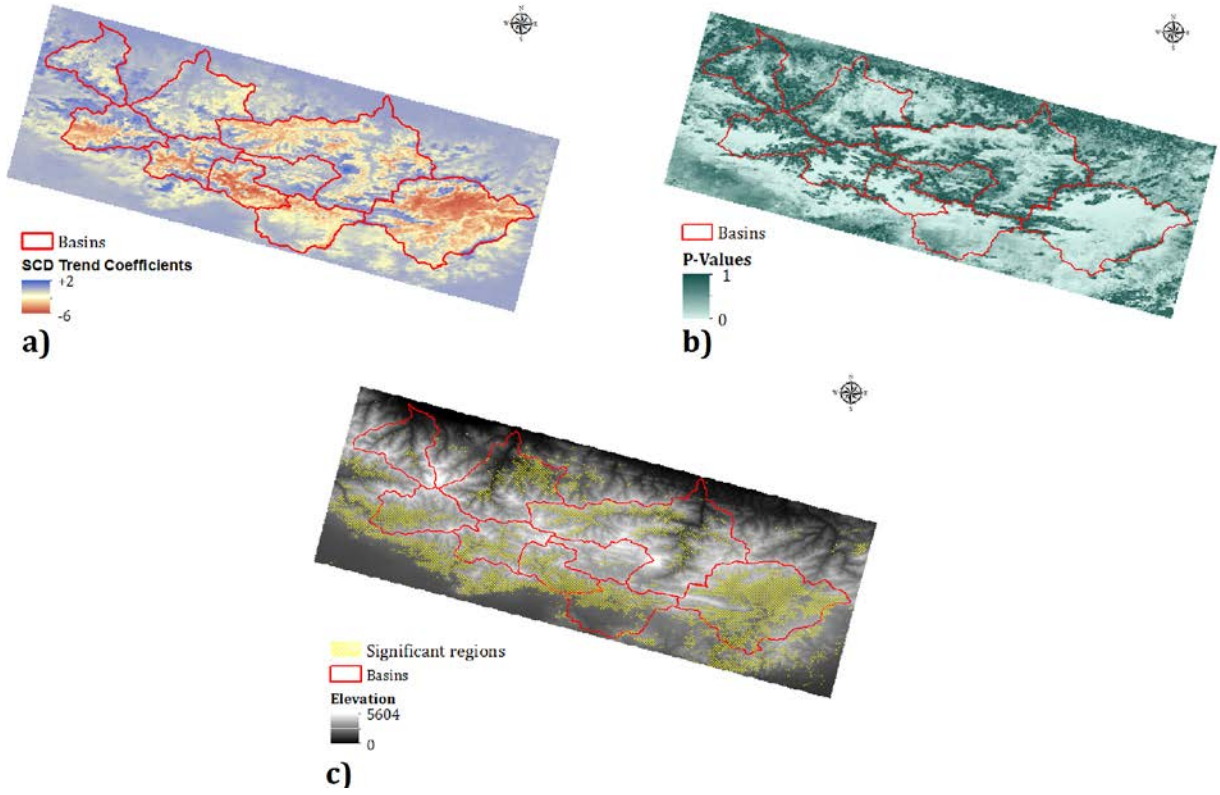


**Figure 8. Snow cover duration trend a) coefficients b) p-values and c) significant areas at 10% level**

Larger areas in southern sub domains where receive lower precipitation have significant SCD changes rather than northern sub domains. Additionally, it seems that areas in mead altitudes are exposed to more variations. To analyze this matter more accurately, significant SCD trend coefficients are plotted against pixel elevations in different aspects (North, East, South, West) and in overall (Fig. 9).

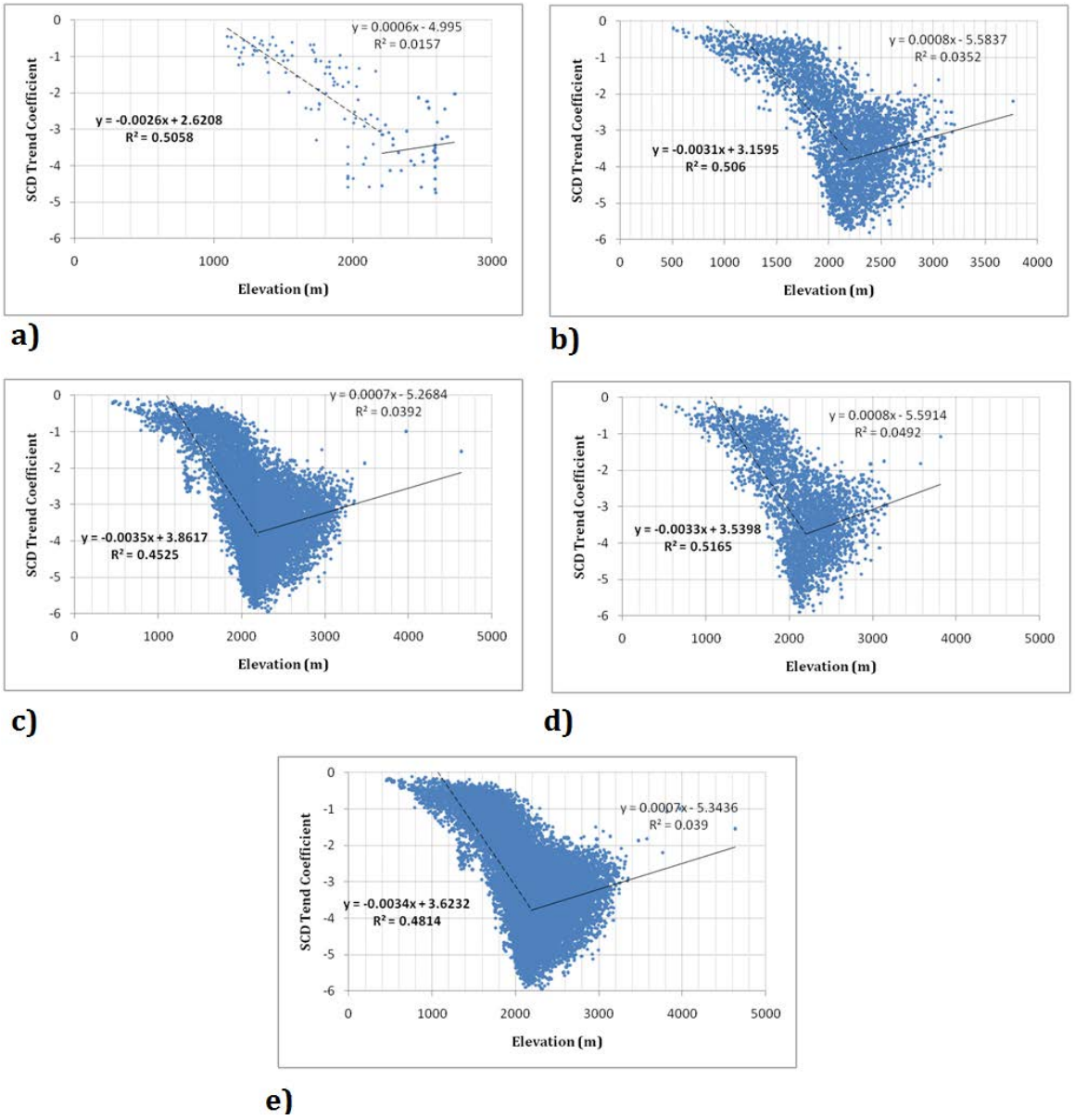


**Figure 9. Snow cover duration trend coefficients and corresponding pixels elevations scatter plot for a) north, b) east c) south d) east and e) all aspects**

As it is shown, in different aspects SCD trend coefficients would reduce as elevation increases until ≈2200 m. a.s.l.. It depicts that snow cover in areas about 2200 m elevation range are reduced more than anywhere else. While SCD trend coefficients have an positive trend in elevations above ≈2200 m. a.s.l.. SCD changes severity is reduced in these areas, although SCD trend coefficients are still negative. It can be explained that temperature decreases with increasing altitude so snow cover sensitivity to temperature variations decreases in higher elevations. In the other words, it may that temperature in areas with 2200 elevation range be about melting threshold. So a slight increase in temperature can cause a considerable snowmelt

there. On the other hand, snow thickness in 2200 elevation range is probably thin in comparison to higher elevations. Therefore, snow cover will respond faster to snow melting and will disappear immediately. Contrasting with lower elevations, in higher altitudes thick snow and low temperature cause that SCD trend coefficients increase along with elevations. This fact is same in all aspects and no significant difference is observed. Elevation histogram of study area pixels, pixels with significant SCD trend coefficients, long-term snow cover percentage in each band and ratio of significant SCD changes to area in each band are presented in figure 10 and table 5.

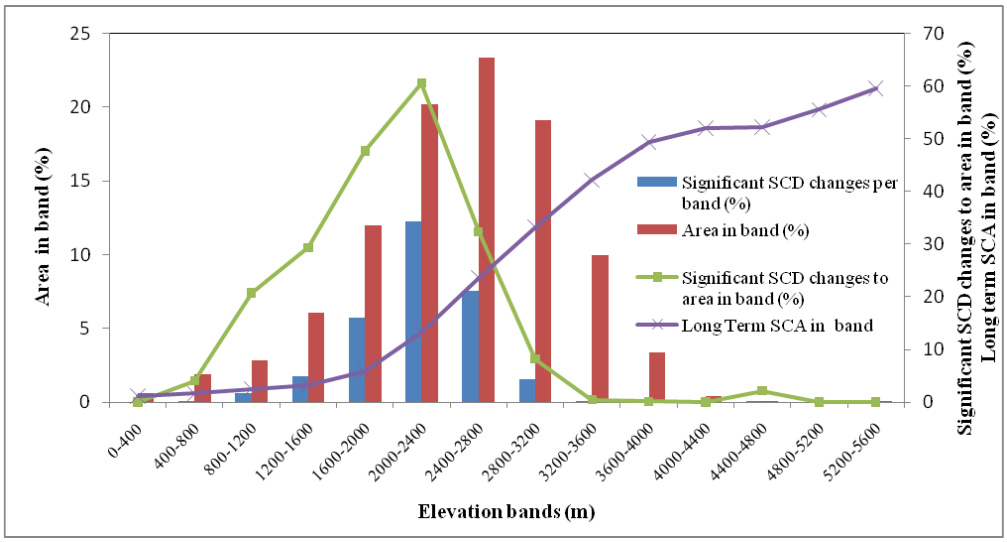


Figure 10. SCD significant coefficients distribution in elevation bands

Table 5. Distribution of snow cover duration trend coefficients in bands

| | Elevation band | 0-400 | 400-800 | 800-1200 | 1200-1600 | 1600-2000 | 2000-2400 | 2400-2800 | 2800-3200 | 3200-3600 | 3600-4000 | 4000-4400 | 4400-4800 | 4800-5200 | 5200-5600 |
|---|---|---|---|---|---|---|---|---|---|---|---|---|---|---|---|
| 1 | **Area in band** | 0.64 | 1.91 | 2.81 | 6.06 | 12.02 | 20.21 | 23.38 | 19.09 | 9.99 | 3.37 | 0.41 | 0.08 | 0.03 | 0.01 |
| 2 | **Significant SCD changes in band (%)** | 0.00 | 0.08 | 0.58 | 1.78 | 5.73 | 12.24 | 7.57 | 1.56 | 0.05 | 0.01 | 0.00 | 0.00 | 0.00 | 0.00 |
| 3 | **Rate of '2' to '1'** | 0.00 | 4.05 | 20.75 | 29.38 | 47.71 | 60.55 | 32.36 | 8.17 | 0.47 | 0.15 | 0.00 | 2.17 | 0.00 | 0.00 |
| 4 | **Long term snow cover in band (%)** | 1.19 | 1.62 | 2.55 | 3.30 | 5.82 | 13.20 | 23.65 | 33.25 | 42.15 | 49.37 | 52.04 | 52.26 | 55.55 | 59.62 |

Red bars show the proportion of areas that are located in corresponding elevation intervals and blue bars similarly represent the percentage of areas with significant SCD changes per elevation band. Hence, the

447 percentage of areas with significant SCD trend coefficients in each band is derived by dividing blue bars to
448 red bars values (green line). It can be found that the 2000-2400 m a.s.l. elevation band is influenced more
449 than the other bands. In the way that 60% of areas in this band have a declining trend during study period.
450 In the meantime, an interesting fact is that the largest elevation band (2400-2800 m as.l.) which individually
451 covers about 23% of entire study area and has a mean SCP about 23% (about 10% more than 2000-2400
452 band) is less affected. Only 32% of areas in this band reveal decrease tendencies, while it was 60% in 2000-
453 2400 m a.s.l. band. This matter is important due to larger area and more snow coverage of 2400-2800 m
454 a.s.l. band. In addition, it can be found that bands above 2800 m a.s.l that have more than 50% SCP are
455 more stable. In which areas with significant SCD trend coefficients are quite rare (less than 10%).

456

457 **4-3- Snow Cover Depletion Curves Derived (SDCs) Metrics**

458 As illustrated in section 3-2, different indexes are extracted from SDCs. These indexes are calculated in
459 every basin individually and considering all basins together. Trend coefficients of defined indexes are given
460 in table 6.

461 **Table 6- Indexes trend coefficients in every basin (*: Significant at 10% level)**

| Index | FiroozKuh | Mamloo | Taleghan | Latian | Karaj | Lar | Haraz | Sehezar | Chaoos | All basins |
|---|---|---|---|---|---|---|---|---|---|---|
| **Maximum snow cover (MSC)** | -2.094* | -1.14* | -1.448* | -0.532 | -2.994* | -0.76* | -0.032* | -2.316* | -0.584* | -1.369* |
| **Snow Accumulation Period (SAP)** | -2.055 | 3.214* | -1.28 | 1.775 | 1.769 | -5.83* | -1.984 | -2.791 | 0.099 | 0.071 |
| **Snow Accumulation Slope (SAS)** | 0.006 | -0.063* | 0.019 | -0.024 | -0.011 | 0.125* | 0.009 | 0.02 | -0.041 | -0.01 |
| **Snow Melt Period (SMP)** | 0.374 | -3.357* | -0.192 | -3.44* | -3.363 | 4.456* | 0.467 | 1.462 | -1.033 | -1.94 |
| **Snow Melt Slope (SMS)** | 0.022 | 0.008 | 0.002 | -0.01 | -0.016* | -0.02* | 0.013 | 0.008 | 0.018 | -0.002 |
| **Maximum Snow Cover Day (MSCD)** | -1.28 | 2.126* | -0.907 | 2.022 | 2.44* | -5.264* | -1.187 | -2.571 | -0.022 | 0.989 |
| **Snow Accumulation Onset Day (SAOD)** | 0.775 | -1.088* | 0.374 | 0.247 | 0.67 | 0.566 | 0.797* | 0.22 | -0.121 | 0.918* |
| **Snow Melt Ending Day (SMED)** | -0.907 | -1.231 | -1.099* | -1.418* | -0.923* | -0.808 | -0.72 | -1.11* | -1.055 | -0.951 |
| **Accumulation-Ablation Period (AAP)** | -1.681 | -0.143 | -1.473* | -1.665 | -1.593* | -1.374* | -1.516* | -1.33 | -0.934 | -1.868* |

462

463 Analysis of trend coefficients leads to following comments:

464 - Maximum snow cover (MSC) was reduced significantly in every basin and all basins except Latian.
465 Maximum trends belong to FiroozKuh and Sehezar basins with -2.994 and -2.316 percent per a
466 year rates, respectively.
467 - Snow accumulation period (SAP) tended to persist longer in Mamloo. This tendency is caused that
468 snow accumulation slope (SAS), which is ratio of MSC to SAP experience a significantly negative
469 trend. In contrast, SAP decreased strongly (≈6 day per a year) in Lar and consequently SAS
470 increased.

- Snow melt period (SMP) shortened of about three days per year in Mamloo and Latian and increased of about 4 days per year in Lar. In addition, snow melt slope (SMS) decreased with -0.016 and -0.02 trend coefficients in Karaj and Lar. Considering SMS definition, Karaj SMP reduction may be inferred by a great reduction in MSC whereas in Lar this situation can be due to SMP elongation.
- Maximum snow cover day (MSCD) was shifted forward in Mamloo and Karaj while was shifted backward in Lar with rate of 5 days per year (from date …. to date … ?). Lar mean hypsometric elevation is 3085 m a.s.l. (Table 1) which is higher than 2800 m a.s.l. elevation. As concluded in past section, areas above this threshold showed low reduction tendency.
- Snow Accumulation was begun faster in Mamloo (Snow accumulation onset day (SAOD) trend coefficient is equal to -1.088). In contrast, snow accumulation was delayed about 0.8 day per year in Haraz, and about 1 day in all basins together.
- Regarding snow melt ending day (SMED) values, Snow melt season was finished about 1 day in each year earlier in Taleghan, Latian, Karaj and Sehezar.
- Accumulation-ablation period that shows entire snow season shows a decreasing tendency in Taleghan, Karaj, Lar, Haraz and considering all basins together. This index varies about 1 to 2 days per a year.

In overall, Lar and Mamloo have most temporal changes in snow coverage condition. As 7 and 6 indexes are changed significantly in Lar and Mamloo respectively. Chaloos has least snow cover variation in time between basins whereas only maximum snow cover showed a slight reduction tendency (-0.584 percent per year).

To measure strength of association between snow cover and temperature variations, Pearson's r and Kendall's tau are computed for pair of derived indexes and averaged monthly LSTs in corresponding duration. Corresponding duration refers to months that are important in indexes formation. For example, maximum snow cover corresponds to autumn until mid of winter temperature. We considered monthly averaged LST in November to February to be corresponded with MSC, SAP, SAS, MSCD and SAOD. Similarly, Averaged temperature in March to June is assumed to be correlated to SMP, SMS and SMED. In addition, for Accumulation-Ablation period (AAP) monthly averaged temperature in December to June is examined. Table 7 represents calculated correlation coefficients in different basins.

**Table 7. Pearson's r and Kendall's tau correlations between derived indexes and land surface temperature (*: Significant at 10% level)**

| Basins | FiroozKuh | | Mamloo | | Taleghan | | Latian | | Karaj | | Lar | | Haraz | | Sehezar | | Chaoos | | All basins | |
|---|---|---|---|---|---|---|---|---|---|---|---|---|---|---|---|---|---|---|---|---|
| Index | R | Tau | R | Tau | R | Tau | R | Tau | R | Tau | R | Tau | R | Tau | R | Tau | R | Tau | R | Tau |
| Maximum snow cover (MSC) | -0.61* | -0.48* | -0.70* | -0.49* | -0.68* | -0.44* | -0.53* | -0.31 | -0.45* | -0.61* | -0.36* | -0.58* | -0.51* | -0.11 | 0 | -0.58* | -0.36* | -0.22 | -0.26 | -0.74* |
| Snow Accumulation Period (SAP) | -0.36 | -0.25 | -0.08 | -0.12 | 0.12 | 0.01 | 0.12 | 0.05 | 0.2 | 0.05 | -0.31 | -0.21 | 0.23 | 0.12 | 0.14 | 0.08 | -0.2 | -0.22 | -0.35 | -0.31 |
| Snow Accumulation Slope (SAS) | -0.06 | 0.03 | 0.07 | 0.01 | -0.14 | -0.14 | -0.24 | -0.15 | -0.4 | -0.32 | 0.28 | 0.19 | -0.18 | -0.09 | -0.26 | -0.25 | 0.18 | 0.1 | 0.05 | 0 |
| Snow Melt Period (SMP) | -0.46* | -0.32* | -0.2 | -0.14 | -0.57* | -0.45* | -0.54* | -0.33 | -0.28 | -0.4* | 0.15 | 0.13 | -0.02 | -0.22 | -0.13 | -0.18 | -0.47* | -0.28 | -0.41 | -0.28 |
| Snow Melt Slope (SMS) | -0.17 | 0 | -0.21 | -0.13 | -0.58* | -0.43* | -0.4 | -0.31 | -0.38 | -0.3 | 0.17 | 0.05 | -0.17 | -0.23 | 0.01 | -0.06 | -0.47* | -0.31 | -0.33 | -0.19 |
| Maximum Snow Cover Day (MSCD) | -0.53* | -0.36* | -0.07 | -0.09 | 0 | -0.04 | 0.16 | 0.04 | 0.04 | -0.04 | -0.25 | -0.1 | 0.21 | 0.09 | 0 | -0.04 | -0.14 | -0.12 | -0.35 | -0.31* |
| Snow Accumulation Onset Day (SAOD) | -0.14 | -0.03 | 0.09 | 0.04 | -0.25 | -0.13 | 0.2 | 0.17 | -0.49* | -0.46* | 0.08 | 0.04 | -0.16 | -0.07 | -0.45* | -0.17 | 0.19 | 0.15 | -0.01 | -0.07 |
| Snow Melt Ending Day (SMED) | -0.91* | -0.69* | -0.67* | -0.47* | -0.41* | -0.13 | -0.71* | -0.44* | -0.43* | -0.42* | -0.57* | -0.58* | -0.8* | -0.54* | -0.19 | -0.34* | -0.6* | -0.53* | -0.79* | -0.51* |
| Accumulation-Ablation Period (AAP) | -0.42 | -0.37* | -0.36 | -0.16 | -0.41 | -0.19 | -0.55* | -0.55* | -0.36 | -0.21 | -0.3 | -0.19 | -0.57* | -0.31 | -0.13 | -0.01 | -0.61* | -0.43* | -0.42* | -0.35* |

Maximum snow cover (MSC) and snow melt ending day (SMED) are the indexes most sensitive to the temperature variations. In which in all basins and considering all basins together, at least one correlation coefficient shows significant co-variability. Moreover, snow melt period (SMP) and accumulation-ablation period (AAP) are significantly correlated with temperature in 5 and 4 basins respectively. Considering all basins together, AAP and MSCD in addition to MSC and SMED are significantly temperature depended.

## 5- Conclusion

The main objective of this study was twofold. First, an innovative methodology is used to reduce cloud obscuration problem in MODIS snow cover products by maintaining snow classification accuracy. Second, we characterized snow cover spatiotemporal changes in study area using different metrics. To do this, 4837 of Terra and Aqua daily snow cover products (MOD10A1 and MYD10A1), 156 of MODIS/Terra monthly land surface Temperature (MOD11C3) and ASTER global digital elevation model were used.

To remove cloud coverage, we implemented a methodology that combines four cloud removal algorithms, including Terra and Aqua combination, time filtering, snowline and neighbor pixels. This methodology was demonstrated effective for removing a large part of the cloud coverage. To maintain accuracy same as original images, we considered methods superiority in months to account temporal excellences. In which methods are prioritized in time and location and applied if was needed to remove clouds in sequence. Using this methodology cloud coverage was dropped under 10% and accuracy was maintained at 93%.

To evaluate snow cover changes, snow cover duration (SCD) and 9 indexes, which were derived from snow cover depletion curves (SDCs) were utilized. The temporal trends of these indexes were analyzed using linear regression. SCD trend coefficients showed to be dependent on altitudes. In the way that SCD trend

coefficients were reduced as elevation increased to about 2200 m a.s.l.. In the other word, until 2200 m a.s.l. negative tendencies in SCD were accelerated. Furthermore, 60% of areas in 2200-2400 m a.s.l. elevation band had significant reduction in SCD while decline in SCD was negligible in elevations above 2800 m a.s.l..

Indexes trend analysis showed significant reduction in maximum snow cover, accumulation-ablation period and a significant forward shift in snow accumulation onset day when all basins be considered together. Also, regarding to evaluation all indexes variations it was found that Lar and Mamloo basins are exposed to most snow cover regime changes while Chaloos basin is less changed in comparison to all studied basins. Investigating co-variability of defined indexes with temperature revealed that temperature has significant influence on maximum snow cover and snow melt ending day over all studied basins. In contrast, snow accumulation period and snow accumulation slope was not sensitive to temperature variations in any basin.

**References:**


Andreadis KM, Lettenmaier DP (2006) Assimilating remotely sensed snow observations into a macroscale hydrology model. Adv Water Resour 29:872–886. doi: 10.1016/j.advwatres.2005.08.004

Ault TW, Czajkowski KP, Benko T, et al (2006) Validation of the MODIS snow product and cloud mask using student and NWS cooperative station observations in the Lower Great Lakes Region. Remote Sens Environ 105:341–353. doi: 10.1016/j.rse.2006.07.004

Bates BC, Kundzewicz ZW, Wu S, Palutikof JP (2008) Climate Change and Water. doi: 10.1016/j.jmb.2010.08.039

Brown R, Derksen C, Wang L (2007) Assessment of spring snow cover duration variability over northern Canada from satellite datasets. Remote Sens Environ 111:367–381. doi: 10.1016/j.rse.2006.09.035

Da Ronco P, De Michele C (2014) Cloud obstruction and snow cover in Alpine areas from MODIS products. Hydrol Earth Syst Sci 18:4579–4600. doi: 10.5194/hess-18-4579-2014

Dozier J (1989) Spectral signature of alpine snow cover from the landsat thematic mapper. Remote Sens Environ 28:9–22. doi: 10.1016/0034-4257(89)90101-6

Dye DG, Tucker CJ (2003) Seasonality and trends of snow-cover, vegetation index, and temperature in northern Eurasia - art. no. 1405. Geophys Res Lett 30:1405–1405. doi: 10.1029/2002GL016384

Frei A, Tedesco M, Lee S, et al (2012) A review of global satellite-derived snow products. Adv Sp Res

50:1007–1029. doi: 10.1016/j.asr.2011.12.021

Gafurov A, Bardossy A (2009) Cloud removal methodology from MODIS snow cover product. Hydrol Earth Syst Sci 13:1361–1373.

Gao Y, Lu N, Yao T (2011) Evaluation of a cloud-gap-filled MODIS daily snow cover product over the Pacific Northwest USA. J Hydrol 404:157–165. doi: 10.1016/j.jhydrol.2011.04.026

Gao Y, Xie H, Yao T, Xue C (2010) Integrated assessment on multi-temporal and multi-sensor combinations for reducing cloud obscuration of MODIS snow cover products of the Pacific Northwest USA. Remote Sens Environ 114:1662–1675. doi: 10.1016/j.rse.2010.02.017

Gascoin S, Hagolle O, Huc M, et al (2015) A snow cover climatology for the Pyrenees from MODIS snow products. Hydrol Earth Syst Sci 19:2337–2351. doi: 10.5194/hess-19-2337-2015

Hall DK, Riggs G a, Digirolamo NE, Bayr KJ (2002) MODIS snow-cover products. Remote Sens Environ 83:88–89. doi: 10.1016/S0034-4257(02)00095-0

Hall DK, Riggs GA (2007) Accuracy assessment of the MODIS snow products. Hydrol Process 21:1534–1547. doi: 10.1002/hyp

Helsel DR, Hirsch RM (2002) Statistical Methods in Water Resources Techniques of Water Resources Investigations. Technometrics. U.S. GEOLOGICAL SURVEY, p 552

Huang X, Hao X, Feng Q, et al (2014) A new MODIS daily cloud free snow cover mapping algorithm on the Tibetan Plateau. Sci Cold Arid Reg 6:116–123. doi: 10.3724/SP.J.1226.2014.00116.A

IPCC (2014) Climate Change 2014: Synthesis Report. International Panel of Climate Chane

IRIMO (2014) Annual Report of of National Crisis Management and Climatic Hazards.

Jin M, Dickinson RE (2010) Land surface skin temperature climatology: benefitting from the strengths of satellite observations. Environ Res Lett 5:044004. doi: 10.1088/1748-9326/5/4/044004

Klein AG, Barnet AC (2003) Validation of daily MODIS snow cover maps of the Upper Rio Grande River Basin for the 2000–2001 snow year. Remote Sens Environ 86:162–176. doi: 10.1016/S0034-4257(03)00097-X

López-Burgos V, Gupta H V., Clark M (2013) Reducing cloud obscuration of MODIS snow cover area products by combining spatio-temporal techniques with a probability of snow approach. Hydrol Earth Syst Sci 17:1809–1823. doi: 10.5194/hess-17-1809-2013

583 Marchane A, Jarlan L, Hanich L, et al (2015) Assessment of daily MODIS snow cover products to monitor
584 snow cover dynamics over the Moroccan Atlas mountain range. Remote Sens Environ 160:72–86.
585 doi: 10.1016/j.rse.2015.01.002

586 Maurer EP, Rhoads JD, Dubayah RO, Lettenmaier DP (2003) Evaluation of the snow-covered area data
587 product from MODIS. Hydrol Process 17:59–71. doi: 10.1002/hyp.1193

588 McGuire M, Wood A, Hamlet A, Lettenmaier D (2006) Use of Satellite Data for Streamflow and Reservoir
589 Storage Forecasts in the Snake River Basin. J Water Resour Plan Manag 132:97–110. doi:
590 10.1061/(ASCE)0733-9496(2006)132:2(97)

591 Mhawej M, Faour G, Fayad A, Shaban A (2014) Towards an enhanced method to map snow cover areas
592 and derive snow-water equivalent in Lebanon. J Hydrol 513:274–282. doi:
593 10.1016/j.jhydrol.2014.03.058

594 Mildrexler DJ, Zhao M, Running SW (2011) A global comparison between station air temperatures and
595 MODIS land surface temperatures reveals the cooling role of forests. J Geophys Res 116:G03025.
596 doi: 10.1029/2010JG001486

597 Mir RA, Jain SK, Saraf AK, Goswami A (2015) Accuracy assessment and trend analysis of MODIS-derived
598 data on snow-covered areas in the Sutlej basin, Western Himalayas. Int J Remote Sens 36:3837–3858.
599 doi: 10.1080/01431161.2015.1070320

600 Mitchell TM (1997) Machine Learning, 1st edn. McGraw-Hill

601 Parajka J, Blöschl G (2006) Validation of MODIS snow cover images over Austria. Hydrol Earth Syst Sci
602 Discuss 3:1569–1601. doi: 10.5194/hessd-3-1569-2006

603 Parajka J, Blöschl G (2008) Spatio-temporal combination of MODIS images - potential for snow cover
604 mapping. Water Resour Res 44:W03406. doi: 10.1029/2007WR006204

605 Parajka J, Pepe M, Rampini a., et al (2010) A regional snow-line method for estimating snow cover from
606 MODIS during cloud cover. J Hydrol 381:203–212. doi: 10.1016/j.jhydrol.2009.11.042

607 Paudel KP, Andersen P (2011) Monitoring snow cover variability in an agropastoral area in the Trans
608 Himalayan region of Nepal using MODIS data with improved cloud removal methodology. Remote
609 Sens Environ 115:1234–1246. doi: 10.1016/j.rse.2011.01.006

610 Shamir E, Georgakakos KP (2014) MODIS Land Surface Temperature as an index of surface air
611 temperature for operational snowpack estimation. Remote Sens Environ 152:83–98. doi:

612 10.1016/j.rse.2014.06.001

613 Statistical Centre of Iran (2010) 2010 population and housing census summury.

614 Tahir AA, Chevallier P, Arnaud Y, et al (2014) Snow cover trend and hydrological characteristics of the
615 Astore River basin (Western Himalayas) and its comparison to the Hunza basin (Karakoram region).
616 Sci Total Environ 505C:748–761. doi: 10.1016/j.scitotenv.2014.10.065

617 Tang Z (2013) Spatiotemporal changes of snow cover over the Tibetan plateau based on cloud-removed
618 moderate resolution imaging spectroradiometer fractional snow cover product from 2001 to 2011. J
619 Appl Remote Sens 7:073582. doi: 10.1117/1.JRS.7.073582

620 Tekeli a. E, Akyürek Z, Arda Şorman a., et al (2005) Using MODIS snow cover maps in modeling
621 snowmelt runoff process in the eastern part of Turkey. Remote Sens Environ 97:216–230. doi:
622 10.1016/j.rse.2005.03.013

623 The World Bank (2007) Making the most of scarcity accountability for better water management in the
624 Middle East and North Africa. World Bank. doi: 10.1596/978-0-8213-6925-8

625 Tong J, Déry SJ, Jackson PL (2008) Topographic control of snow distribution in an alpine watershed of
626 western Canada inferred from spatially-filtered MODIS snow products. Hydrol Earth Syst Sci Discuss
627 5:2347–2371. doi: 10.5194/hessd-5-2347-2008

628 Van Nguyen O, Kawamura K, Trong DP, et al (2015) Temporal change and its spatial variety on land
629 surface temperature and land use changes in the Red River Delta, Vietnam, using MODIS time-series
630 imagery. Environ Monit Assess 187:464. doi: 10.1007/s10661-015-4691-3

631 Wang R, Yao Z, Liu Z, et al (2015) Snow cover variability and snowmelt in a high-altitude ungauged
632 catchment. Hydrol Process 29:3665–3676. doi: 10.1002/hyp.10472

633 Wang W, Huang X, Deng J, et al (2014a) Spatio-Temporal Change of Snow Cover and Its Response to
634 Climate over the Tibetan Plateau Based on an Improved Daily Cloud-Free Snow Cover Product.
635 Remote Sens 7:169–194. doi: 10.3390/rs70100169

636 Wang X, Xie H, Liang T, Huang X (2009) Comparison and validation of MODIS standard and new
637 combination of Terra and Aqua snow cover products in northern Xinjiang , China. Hydrol Process
638 23:419–429. doi: 10.1002/hyp.7151

639 Wang X, Zheng H, Chen Y, et al (2014b) Mapping snow cover variations using a MODIS daily cloud-free
640 snow cover product in northeast China. J Appl Remote Sens 8:084681. doi: 10.1117/1.JRS.8.084681

641 Yang J, Jiang L, Ménard CB, et al (2015) Evaluation of snow products over the Tibetan Plateau. Hydrol
642 Process 29:3247–3260. doi: 10.1002/hyp.10427

643